Journal of Alloys and Compounds 509 (2011) 4314–4319

Contents lists available at ScienceDirect

Journal of Alloys and Compounds

journal homepage: www.elsevier.com/locate/jallcom

Thermal, structural and magnetic properties of some zinc phosphate glasses doped with manganese ions

Petru Pascuta[a,*], Maria Bosca[a], Gheorghe Borodi[b], Eugen Culea[a]

[a] Physics Department, Technical University, 400020 Cluj-Napoca, Romania
[b] National Institute for R&D of Isotopic and Molecular Technologies, P.O. Box 700, RO-400293 Cluj-Napoca, Romania

ARTICLE INFO

Article history:
Received 4 September 2010
Received in revised form 4 January 2011
Accepted 7 January 2011
Available online 15 January 2011

Keywords:
Zinc phosphate glasses
Manganese ions
Magnetic properties
EPR
DTA

ABSTRACT

$(MnO)_x\cdot(P_2O_5)_{40}\cdot(ZnO)_{60-x}$ glasses containing different concentrations of MnO ranging from 0 to 20 mol% were prepared by the melt-quenching technique. The samples had a fixed P_2O_5 content of 40 mol% and the MnO:ZnO ratio was varied. The thermal, structural and magnetic properties of these glasses were investigated by means of differential thermal analysis (DTA), electron paramagnetic resonance (EPR) and magnetic susceptibility measurements. Compositional dependence of the glass transition (T_g), crystallization (T_p) and melting temperatures were determined by DTA investigations. From the dependence of the T_g on the heating rate (a), the activation energy of the glass transition (E_g) was calculated. The fragility index (F) for the studied glasses was determined to see whether these materials are obtained from kinetically strong-glass-forming (KS) or kinetically fragile-glass forming (KF) liquids. The EPR spectra of the studied glasses revealed absorptions centered at $g\approx2.0$, 3.3 and 4.3. The compositional variations of the intensity and line width of these absorption lines was interpreted in terms of the variation in the concentration of the Mn^{2+} and Mn^{3+} ions in the glass and the interaction between the manganese ions. EPR and magnetic susceptibility data reveal that both Mn^{2+} and Mn^{3+} ions are present in the studied glasses, their relative concentration being dependent on the glass composition. Magnetic susceptibility data reveal an antiferromagnetic interaction between the manganese ions for the glasses containing 20 mol% MnO.

1. Introduction

Glasses containing transition metal ions (TMI) have attracted much attention due to their electrical [1–7], optical [8–13] and magnetic properties [14–17] which render them suitable for large practical and potential applications in many fields such as memory switching [18,19] electronics [5,6,12,15], catalysis [20–22] and magnetic information storage [10,14,16]. These properties of the TMI glasses arise from the presence of TMI in multivalent states [4,23–26]. Manganese ions have been frequently used as paramagnetic probes for exploring the structure and properties of glasses [27–33]. Studies of the coordination, bonding characteristics and covalence state of TMI in glasses are very helpful in understanding the structure of the glassy state. Changes in the chemical composition of glass may change the local environment of the TMI incorporated into the glass, leading to ligand field changes which may be reflected in the EPR spectra [34]. EPR studies of manganese ions in glasses have been used to obtain information regarding the glass network and to identify the site symmetry around the manganese ions [27–36]. Manganese ions exist in different valence states with different local symmetry in the glasses, for example, as Mn^{2+} with both tetrahedral and octahedral coordination and/or as Mn^{3+} with octahedral coordination [31,35]. The content of manganese in different coordinations and valence states exist in the glass depending upon the quantitative properties of modifiers and glass formers, size of the ions in the glass structure, their field strength, mobility of the modifier cation, etc. [31,35]. Though Mn^{2+} and Mn^{3+} ions are both paramagnetic, only Mn^{2+} ($3d5$, $^6S_{5/2}$) shows EPR absorptions at room temperature. It is well known that in case of d^5 metal ions, the axial distortion of octahedral symmetry gives rise to three Kramers doublets $\left|\pm5/2\right\rangle$, $\left|\pm3/2\right\rangle$ and $\left|\pm1/2\right\rangle$. An application of Zeeman field will split the spin degeneracy of the Kramers doublets. As the crystal field splitting is normally much greater than the Zeeman field, the resonances observed are due to transitions within the Kramers doublets split by the Zeeman field [29]. Generally, the spectra consist of resonance lines centered at $g\approx2.0$, 3.3 and 4.3 with their relative intensity being strongly dependent on composition.

Magnetic susceptibility measurements of glasses containing manganese ions reveal the nature of interactions between the manganese ions apart from providing information on the valence states of manganese ions. The magnetic properties of glasses containing manganese depend on the concentration of the 3d element and the ratio of valence states as well as on the structure of the vitre-

* Corresponding author. Tel.: +40 264 401 262; fax: +40 264 595 355.
E-mail address: petru.pascuta@phys.utcluj.ro (P. Pascuta).

0925-8388/$ – see front matter © 2011 Elsevier B.V. All rights reserved.
doi:10.1016/j.jallcom.2011.01.056

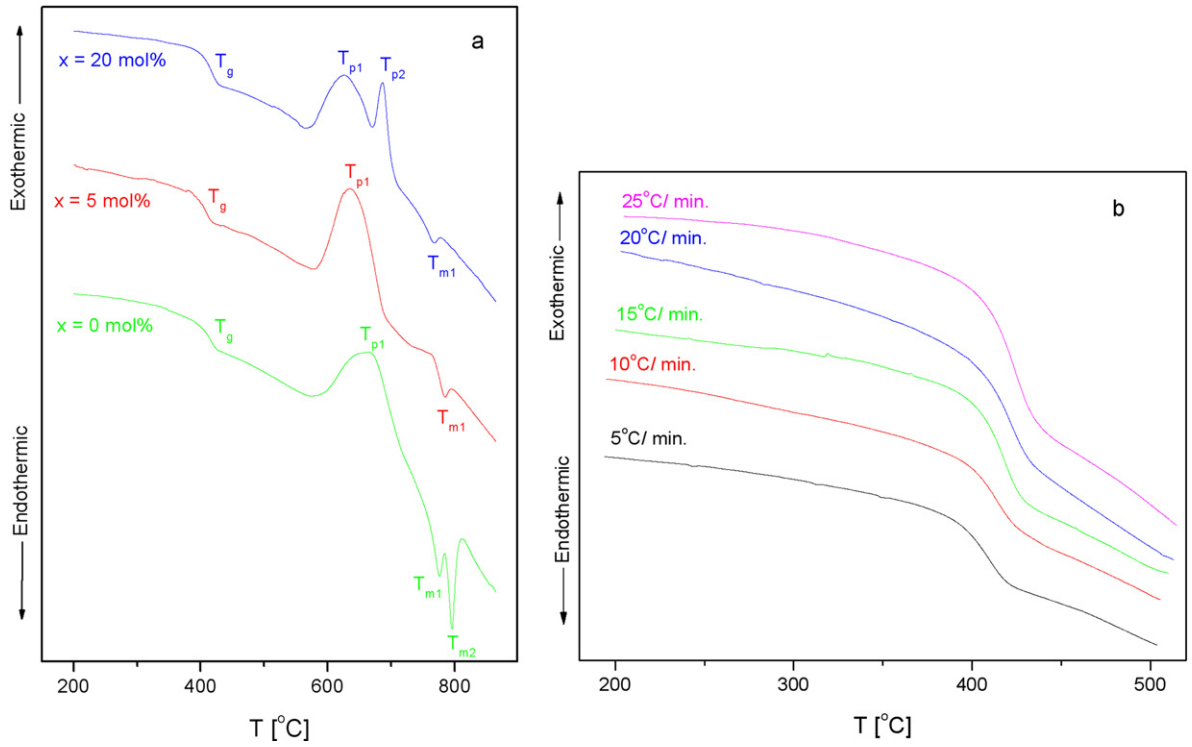

Fig. 1. DTA curves of $(MnO)_x{\cdot}(P_2O_5)_{40}{\cdot}(ZnO)_{60-x}$ glasses at the heating rate of 15 °C/min (a) and DTA curves obtained with different heating rates for glasses containing 10 mol% MnO (b).

ous matrix and implicitly on the conditions of sample preparation. The superexchange interaction of the manganese ions in the oxide glasses has been mostly attributed to an antiferromagnetic coupling within the pairs Mn^{2+}–Mn^{2+}, Mn^{2+}–Mn^{3+} and Mn^{3+}–Mn^{3+} [33,37–39].

The aim of this paper is to present our results obtained by means of DTA, EPR and magnetic susceptibility measurements performed on some zinc phosphate glasses gradually doped with manganese ions. The research is part of a comparative analysis program focused on the behaviour of TMI in vitreous matrices, in order to obtain generally valuable rules, which allow imposing and controlling the properties of such materials.

2. Experimental

Glasses in the ternary system $(MnO)_x{\cdot}(P_2O_5)_{40}{\cdot}(ZnO)_{60-x}$ with x varying from 0 mol% to 20 mol% were prepared by conventional melt-quenching using as starting materials reagent grade MnO, P_2O_5 and ZnO of high purity (99.9%) in suitable proportion. The mechanically homogenized mixtures were melted in sintered corundum crucibles at 1100 °C in an electric furnace. The samples were put into the electric furnace directly at this temperature. After 10 min the molten material was quenched at room temperature by pouring onto a stainless-steel plate. The obtained samples were analyzed by means of X-ray diffraction. The patterns obtained are characteristic for vitreous systems in this concentration range ($0 \le x \le 20$ mol%) of MnO [40].

The thermal behaviour of glass samples was carried out using a PerkinElmer TG/DTA 6300 thermal analyzer under Ar gas atmosphere. About 20 mg of bulk glass was heated in Pt-holder with another Pt-holder containing α-alumina as a reference material. In order to determine the activation energy of the glass transition and activation energy for the crystallization process the DTA traces were recorded at five heating rates a = 5, 10, 15, 20 and 25 °C/min.

The EPR measurements of powder samples were carried out in the X-band (~9.79 GHz) at room temperature using a Bruker E-500 ELEXSYS spectrometer. The spectra processing was performed by the Bruker Xepr software. To avoid the alteration of the glass structure due to the ambient conditions, especially humidity, samples were poured immediately after preparation and enclosed in tubular holders of the same caliber. Equal quantities of samples were studied.

The magnetic susceptibility measurements were made using a Faraday type magnetic balance in 80–300 K temperature range. Corrections due to the diamagnetism of the MnO, P_2O_5 and ZnO and were taken into account in order to obtain the real magnetic susceptibility of manganese ions in the studied glasses.

3. Results and discussion

3.1. DTA data

DTA is very suitable for determination of glass characteristic temperatures, such as glass transition temperature, T_g, crystallization temperature, T_p and melting temperature, T_m. These thermal parameters are suitable for a qualitative estimation of the thermal stability of glasses and the glass forming ability. Typical DTA curves for $MnO–P_2O_5–ZnO$ glasses at a heating rate of 15 °C/min are shown in Fig. 1a. The obtained thermal parameters are summarized in Table 1. The appearance of a single peak due to T_g in the DTA pattern of all the glasses indicates the homogeneity of the studied glasses. One also observes that T_g for all samples is around 415 °C, denoting that T_g in this zinc phosphate glass matrix is poorly affected by the substitution of ZnO with MnO up to 20 mol%.

The thermal stability (TS) of glass can be expressed by the temperature difference between the T_g and T_c introduced by Dietzel [41–44]:

$$TS = T_c - T_g, \quad (1)$$

where T_c is the onset temperature of crystallization. By the use of the characteristic temperatures, Hruby [45,46] introduce the glass forming ability (K_{gl}) which is defined by the relation:

$$K_{gl} = \frac{(T_c - T_g)}{(T_m - T_c)} \quad (2)$$

Another parameter usually employed to estimate the glass stability, introduced by Saad and Poulin [47] is the thermal stability parameter (S):

$$S = \frac{(T_p - T_c)(T_c - T_g)}{T_g}, \quad (3)$$

which reflects the resistance to divitrification after formation of the glass. In Eq. (3), the $(T_p - T_c)$ term is related to the rate of devitrification transformation of the glassy phase. On the other hand, the

Table 1
Glass transition temperature (T_g), crystallization temperatures (T_{p1} and T_{p2}), melting temperatures (T_{m1} and T_{m2}), thermal stability (TS, K_{gl} and S), fragility index (F) and activation energy of glass transition (E_g) for the $(MnO)_x\cdot(P_2O_5)_{40}\cdot(ZnO)_{60-x}$ glasses.

x [mol%]	T_g [±1 °C]	T_{p1} [±1 °C]	T_{p2} [±1 °C]	T_{m1} [±1 °C]	T_{m2} [±1 °C]	TS [±1 °C]	K_{gl} [±0.05]	S [±1 °C]	F [±0.5]	E_g [±5 kJ/mol]
0	412	667	–	776	796	195	0.85	35.67	20.16	264.38
5	407	635	–	785	–	163	0.76	26.03	21.01	273.53
10	417	629	–	782	–	151	0.71	22.09	27.12	358.33
20	415	625	686	767	–	144	0.69	22.90	28.91	380.78

higher values of the $(T_c - T_g)$ term delays the nucleation process [42,44]. The obtained values of TS, K_{gl} and S for different content of manganese ions are given in Table 1. Inspecting these data, one remarks that the glass matrix (undoped with MnO) has the highest thermal stability as indicated by all glass stability parameters. The glasses containing 20 mol% MnO shows a tendency towards crystallization more than the other compositions.

The fragility index can be obtained using the following relationship [42,44,48,49]:

$$F = \frac{E_g}{RT_g \ln 10}, \quad (4)$$

where E_g is the activation energy of glass transition. The activation energy of enthalpy relaxation of the glass transition, or the activation energy of glass transition E_g of the investigated glasses, was calculated using the Kissinger formula [50]:

$$\ln\left(\frac{T_g^2}{a}\right) = \frac{E_g}{RT_g} + \text{const.} \quad (5)$$

where a is the heating rate of DTA (a = 5, 10, 15, 20 and 25 °C/min), T_g is the glass transition at different heating rates and R is the gas constant. DTA curves obtained with different heating rates for glasses containing 10 mol% MnO are shown in Fig. 1b. The plot of $\ln(T_g^2/a)$ versus $1000/T_g$ is expected to be linear. The glass transition activation energy, E_g, can be calculated from the slop of this plot. Fig. 2 shows the plots of $\ln(T_g^2/a)$ versus $10^3/T_g$ for different contents of MnO. The values of the fragility index and of the activation energy of glass transition obtained for the studied glasses are shown in Table 1. The study of structural relaxation in the glass transition region of glass-forming liquids is important from both academic and technological points of view. Structural relaxation processes in glasses occur at temperatures lower than their T_g. Glass forming liquids that exhibit an approximately Arrhenius temperature dependence of the viscosity are defined as strong glass formers and those which exhibit a non-Arrhenius behaviour are declared fragile glass former [42–44]. Fragile glasses have higher ionic bond character as compared to covalent bond component. Strong glasses are those which show resistance to structural degradation in the liquid state. It was found that the limit for kinetically strong-glass-forming (KS) liquids is reached for a low value of F ($F \approx 16$) [42,44,51], while the limit for kinetically fragile-glass-forming (KF) liquids is characterized by a high value of F ($F \approx 200$) [42,44]. For the $(MnO)_x\cdot(P_2O_5)_{40}\cdot(ZnO)_{60-x}$ ($0 \le x \le 20$ mol%) glasses the values of F are near to KS limit (Table 1). This indicates that all the glassy alloys prepared in the present study are obtained from KS liquids.

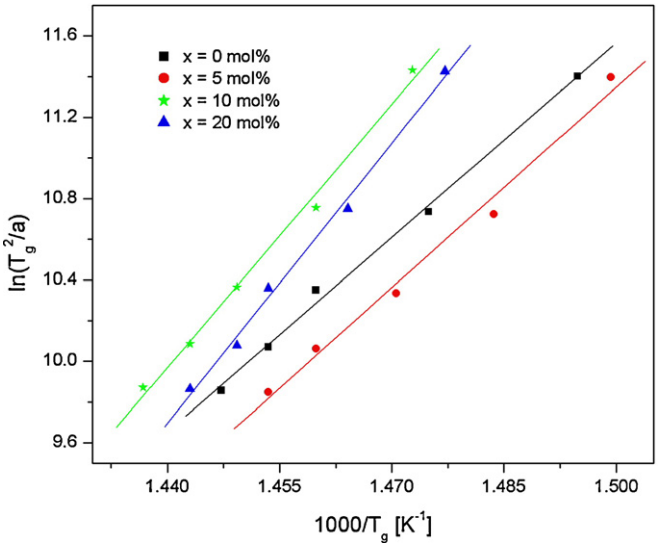

Fig. 2. Plots of $\ln(T_g^2/a)$ versus $1000/T_g$ for the $(MnO)_x\cdot(P_2O_5)_{40}\cdot(ZnO)_{60-x}$ glasses.

3.2. EPR data

For exploring the local structure of the studied glasses, Mn^{2+} ($3d5, {}^6S_{5/2}$) ions were chosen as paramagnetic probes in EPR measurements. The absorption spectra are sensitive to the symmetry of the structural units which are building up the glass network and give information about the involved paramagnetic ions, valence states and interactions. The EPR spectra obtained at room temperature for the $(MnO)_x\cdot(P_2O_5)_{40}\cdot(ZnO)_{60-x}$ glass system with $1 \le x \le 20$ mol% are shown in Fig. 3. As can be seen from this figure, there is a strong dependence of the absorption spectra structure and parameters on the MnO content of the samples. The EPR spectra structure consists mainly in absorptions centered at $g \approx 2.0$, 3.3 and $g \approx 4.3$ their prevalence depending on manganese ions concentrations. The resonance at $g \approx 2.0$ is attributed in general to (i) isolated Mn^{2+} ions in octahedral symmetric sites slightly tetragonally distorted when the hyperfine structure (hfs) is resolved or to (ii) associated ones, the Mn^{2+} ions being involved in dipole–dipole and/or superexchange interactions, and is known to arise from the transition between the energy levels of the lower doublet $|\pm 1/2\rangle$ [30,32,33,52–54]. At low content of manganese ions (x = 1 mol%), the EPR spectrum shows a hfs sextet due to the hyperfine interaction of the electron spin ($S = 5/2$) with its own nuclear spin ($I = 5/2$) superposed on a large absorption line for $g \approx 2.0$. The g-factor value and the well resolved hfs with a coupling constant of $A \approx 95$ G show the predominantly ionic character of the bonding between Mn^{2+} and the O^{2-} ions generating the octahedral symmetry of the ligand field. Weak axial distortions could be superposed on this field, varying in intensity and orientation from the vicinity of a manganese ion to another [54,55]. When the concentration of manganese ions increased beyond 1 mol%, the hfs sextet dissappears leaving behind a single broad line due to both the distribution of crystal field parameters and the dipole–dipole interaction accompanied by the superexchange magnetic interaction. The resonances at $g \approx 3.3$ and 4.3 are due to magnetically isolated Mn^{2+} ions located at tetragonally distorted sites of octahedral symmetry subjected to strong crystal field effects and arise from transitions between the energy levels of the middle Kramers doublet $|\pm 3/2\rangle$ [30,32,33,54]. In the case of our glasses these absorptions are less intense than the one at $g \approx 2.0$ and appear only for low concentrations of manganese ions ($x \le 5$ mol%). The resonance signal centered at $g \approx 3.3$ is broad, unresolved, with the aspect of a shoulder like signal. There is a relatively small concentration of Mn^{2+} ions involved in such structural units.

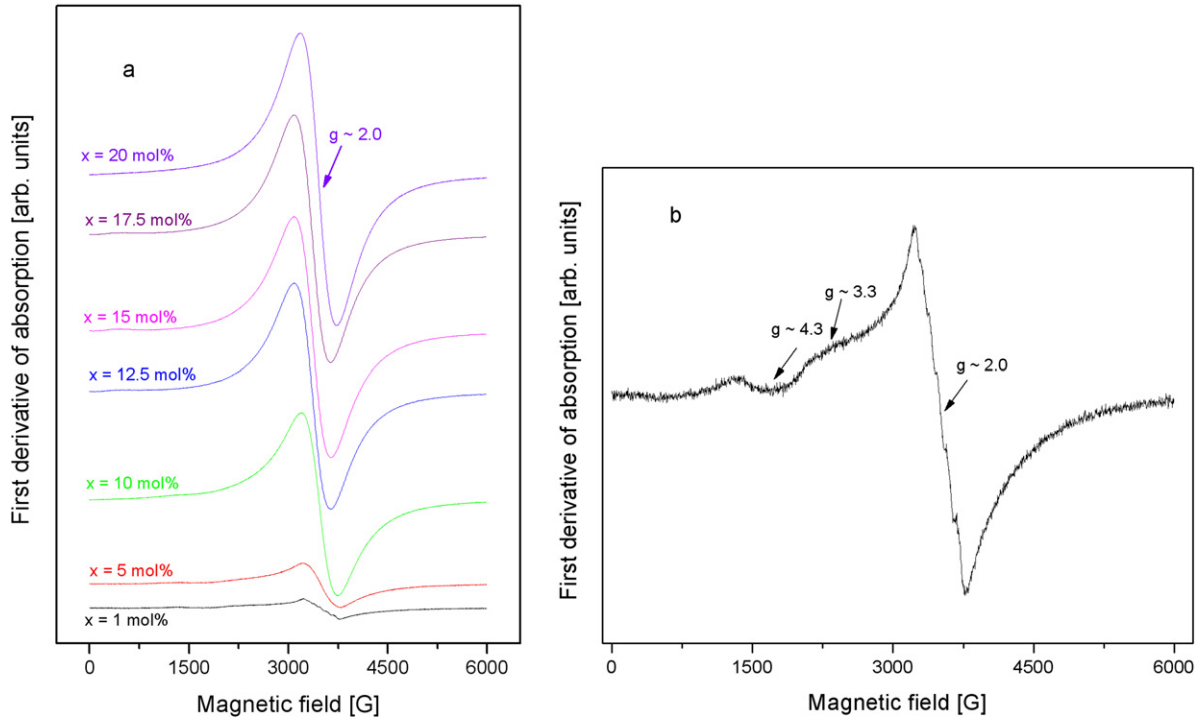

Fig. 3. EPR spectra of Mn^{2+} ions in the $(MnO)_x{\cdot}(P_2O_5)_{40}{\cdot}(ZnO)_{60-x}$ glasses (a) and EPR spectra of glasses containing 1 mol% MnO (b).

The lack of hfs at these absorption lines could be due to the fluctuations of the ligand field parameters in the Mn^{2+} ion neighborhood and the random distribution of the octahedral distortions vicinity. The evolution of the resonance line centered at $g \approx 2.0$ with increasing of manganese ions content was followed with respect to the EPR characteristic parameters, namely the absorption line intensity (J) and the peak-to-peak linewidth (ΔH). The corresponding variations of these parameters versus the manganese ions content are plotted in Fig. 4. The intensity and line-width of the $g \approx 2.0$ absorption line increase as function of the manganese ions content. Generally, the signal intensity is proportional to the number of EPR active species involved in the resonance absorption, so the increase of the $g \approx 2.0$ line intensity indicates an increase in Mn^{2+} ion concentration. The nonlinear increase of J and ΔH with the increase of the MnO concentration (depicted in Fig. 2) can be attributed to the process by which the manganese ions enter the vitreous glass matrix either as Mn^{2+} or Mn^{3+} [30,54,56–58]. Without giving rise to EPR absorption, Mn^{3+} ions may influence the Mn^{2+} ions absorption spectra when they are involved in magnetic interactions. The $\Delta H = f(x)$ dependence reflects the competition between the broadening mechanisms (due to the dipole–dipole interactions, the increased disordering of the matrix structure, the interactions between ions in multivalent states) and the narrowing ones (due to the superexchange interactions within the pairs of manganese ions). These mechanisms act simultaneously but one of them may become predominant in function of the MnO content of the samples. Following the $\Delta H = f(x)$ dependence it was observed a deviation from linearity at $x > 10$ mol%. This suggests that for $x > 10$ mol% superexchange interactions narrow the resonance line from $g \approx 2$.

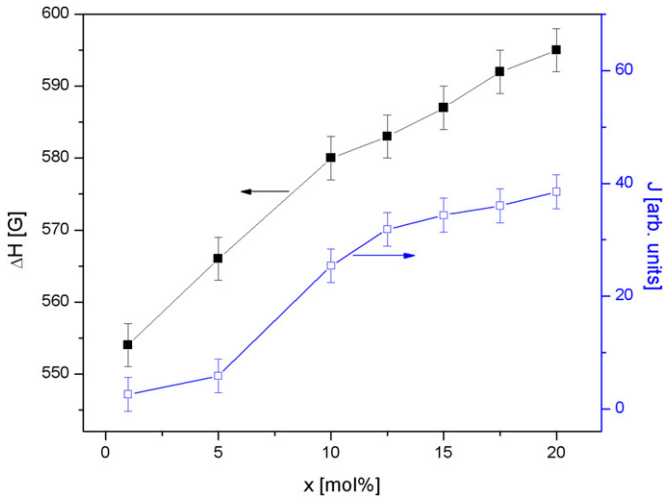

Fig. 4. Composition dependence of intensity and line-width for $g \approx 2.0$ absorption line of $(MnO)_x{\cdot}(P_2O_5)_{40}{\cdot}(ZnO)_{60-x}$ glasses. The lines are drawn as a guide for the eyes.

3.3. Magnetic susceptibility data

The magnetic susceptibility data correlate well with the EPR results and also complete them. The magnetic susceptibility data offered useful information concerning the distribution of the manganese ions in the host glass matrix, the valence state of manganese ions and the nature of the magnetic interactions between these ions in various composition ranges. The temperature dependence of the reciprocal magnetic susceptibility of glasses from the studied system is presented in Fig. 5. For the samples with $x \leq 10$ mol % a Curie law is observed which is typical for isolated ions or/and subjected to dipole–dipole interactions. For $x > 10$ mol% the reciprocal magnetic susceptibility follows the Curie–Weiss law:

$$\chi = \chi_0 + \frac{C_M}{T - \theta_p} \tag{6}$$

where χ_0 is the temperature-independent contribution, θ_p is the paramagnetic Curie temperature and C_M is the molar Curie constant

$$C_M = \frac{\mu_{eff}^2 \cdot N_A}{3k_B} \tag{7}$$

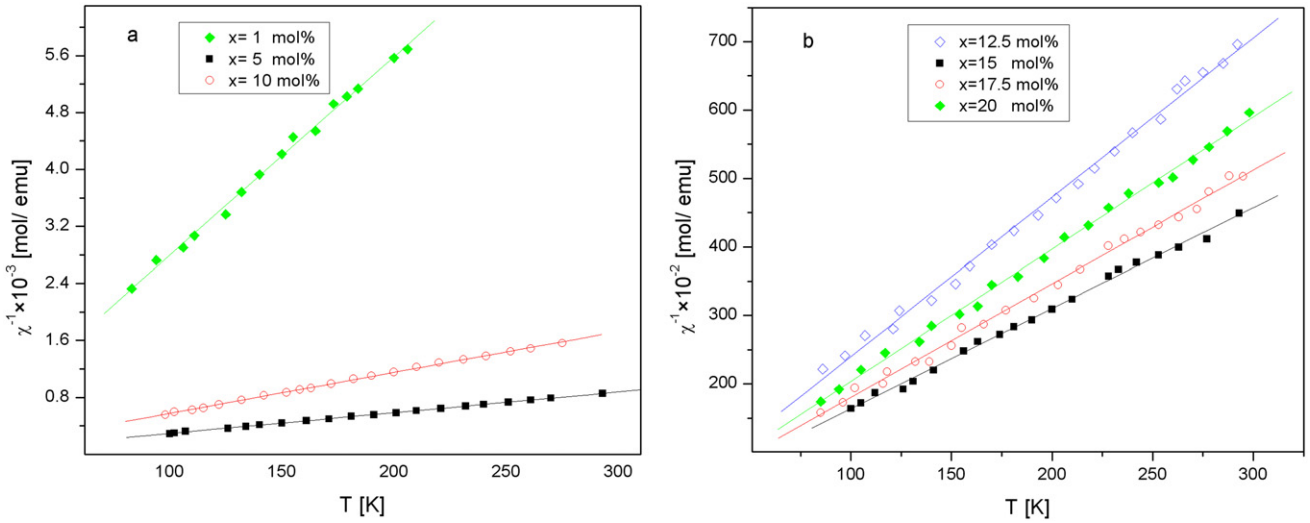

Fig. 5. Temperature dependence of the reciprocal magnetic susceptibility for $(MnO)_x\cdot(P_2O_5)_{40}\cdot(ZnO)_{60-x}$ glasses with $1 \le x \le 10$ mol % (a) and with $12.5 \le x \le 20$ mol % (b).

In this formula, μ_{eff} is the effective magnetic moment, N_A is the Avogadro's number, x is the concentration of manganese ions in the glass, k_B is the Boltzmann's constant. The negative values of θ_p obtained for the glasses with $x > 10$ mol% indicate that the manganese ions are coupled by antiferromagnetic interactions, namely superexchange ones. The θ_p is a rough indicator of both the strength of the interaction between the magnetic moments and the number of magnetic ions participating in the interactions. The absolute magnitude of θ_p values increases with increasing the MnO content, x, suggesting that the magnetic interactions become stronger at higher x values (Fig. 6). Due to the disordered structure of glasses, the magnetic order takes place at short range, possibly in the form of the micromagnetic type order [59]. The values of the effective magnetic moment of manganese ions in the studied samples were estimated using the formula:

$$\mu_{eff} = 2.827\sqrt{\frac{C_M}{x}} \tag{8}$$

The values obtained for μ_{eff} and C_M are given in Table 2. For all the studied glasses the experimental values obtained for C_M and, consequently, for μ_{eff} are lower than those which correspond to the MnO content, considering that all manganese ions are in the Mn^{2+} valence state, but they are higher than those calculated for the case when all manganese ions would appear as Mn^{3+} species (Table 2). Therefore we consider that in these glasses are present both Mn^{2+} and Mn^{3+} ions. Having in view this supposition and using the atomic magnetic moment values of the free Mn^{2+} and Mn^{3+} ions, and $\mu_{Mn^{3+}} = 4.90\mu_B$ [60], we can estimate in first approximation the molar fraction of these ions in the investigated glasses using the relations:

$$x\cdot\mu_{eff}^2 = x_1\cdot\mu_{Mn^{2+}}^2 + x_2\cdot\mu_{Mn^{3+}}^2 \quad \text{and} \quad x = x_1 + x_2, \tag{9}$$

where x_1 and x_2 are the molar fraction of manganese ions in Mn^{2+} and Mn^{3+} valence states. The results obtained are listed in Table 2. From these data one remarks that the molar fraction of both Mn^{2+} and Mn^{3+} ions increases with increasing the content of MnO in whole concentration range. For all the studied glasses the molar

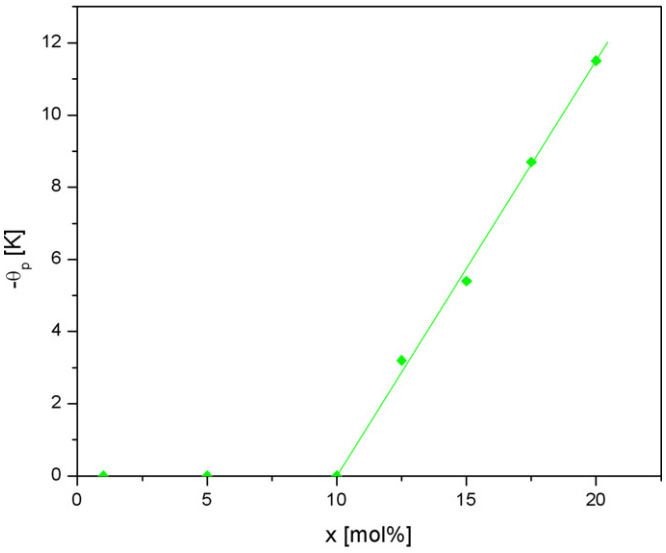

Fig. 6. The composition dependence of the paramagnetic Curie temperature for $(MnO)_x\cdot(P_2O_5)_{40}\cdot(ZnO)_{60-x}$ glasses. The solid line is only a guide for the eye.

Table 2
Molar Curie constant C_M, experimental values of μ_{eff}, the molar fraction of Mn^{2+} ions (x_1), the molar fraction of Mn^{3+} ions (x_2) and the x_2/x_1 ratio for $(MnO)_x\cdot(P_2O_5)_{40}\cdot(ZnO)_{60-x}$ glasses.

x [mol%]	C_M [$\pm 1\times10^{-4}$ emu K/mol]	μ_{eff} [$\pm 1\times10^{-2}\mu_B$]	x_1 [±0.1 mol %]	x_2 [±0.1 mol %]	x_2/x_1 [±0.1]
1	0.0358	5.35	0.4	0.6	1.50
5	0.1739	5.27	1.7	3.3	1.94
10	0.3431	5.23	3	7	2.33
12.5	0.4301	5.24	3.9	8.6	2.21
15	0.5178	5.25	4.8	10.2	2.13
17.5	0.6029	5.24	5.5	12	2.18
20	0.6813	5.22	5.9	14.1	2.34

fraction of Mn^{2+} ions are lower than that of the molar fraction of Mn^{3+} ions. The ratio of the number of ions in Mn^{3+} state (x_2) and the number of ions in Mn^{2+} state (x_1) for studied glasses is listed in Table 2. The x_2/x_1 ratio increases with the increasing of MnO content more prominently for $x \leq 10$ mol %. This is due to a decrease in Mn^{3+} and a corresponding increase in Mn^{2+} up to a certain level ($x = 10$ mol%) after that which there are not many changes.

4. Conclusions

Glasses of the $(MnO)_x \cdot (P_2O_5)_{40} \cdot (ZnO)_{60-x}$ system were obtained within a large concentration range, namely $0 \leq x \leq 20$ mol%. DTA data show that the glass undoped with MnO (the host glass matrix) has the highest thermal stability. The values of F indicate that the studied glasses are formed from KS liquids. The values calculated for the activation energy are ranging from 264.38 to 380.78 kJ/mol by the progressive addition of manganese ions in the investigated composition range. The DTA data indicate a good thermal stability of the studied glasses. EPR absorption spectra due to Mn^{2+} ions were detected within $1 \leq x \leq 20$ mol %. The structure of the EPR spectra and the values of the EPR parameters of resonance lines strongly depend of the manganese ion concentrations. The analysis of the EPR spectra shows that they are due to isolated Mn^{2+} ions in octahedral symmetric sites slightly tetragonally distorted when the hfs is resolved or to associated ones, when the Mn^{2+} ions are involved in dipole–dipole and/or superexchange interactions giving rise to an absorption line centered at $g \approx 2.0$. Strongly distorted versions of these sites result in the resonance lines at $g \approx 4.3$ and 3.3. The intensity of the last two lines is small enough and indicates a relative low concentration of Mn^{2+} ions involved in such structural units. The magnetic susceptibility data revealed superexchange magnetic interactions involving manganese ions, antiferromagnetically coupled for the sample containing 20 mol% MnO. Manganese ions enter the studied glasses in both Mn^{2+} and Mn^{3+} valence states, the last being the dominating one.

Comparing the results obtained in this paper for the $(MnO)_x \cdot (P_2O_5)_{40} \cdot (ZnO)_{60-x}$ glasses with the ones obtained by studying the $(Fe_2O_3)_x \cdot (P_2O_5)_{40} \cdot (ZnO)_{60-x}$ glasses [17], we note that both systems show a similar magnetic behaviour.

Acknowledgement

This work was supported by CNCSIS–UEFISCSU, project number PNII–IDEI 226/2008.

References

[1] A. Ghosh, Phys. Rev. B 42 (1990) 5665.
[2] A. Ghosh, Phys. Rev. B 41 (1990) 1479.
[3] I. Ardelean, P. Pascuta, Mod. Phys. Lett. B 15 (2001) 1445.
[4] S. Bhattacharya, A. Ghosh, Phys. Rev. B 68 (2003) 224202.
[5] T. Sankarappa, G.B. Devidas, M.P. Kumar, S. Kumar, B.V. Kumar, J. Alloys Compd. 469 (2009) 576.
[6] A.A. Bahgat, B.A.A. Makram, E.E. Shaisha, M.M. El-Desoky, J. Alloys Compd. 506 (2010) 141.
[7] K. Srilatha, K. Sambasiva Rao, Y. Gandhi, V. Ravikumar, N. Veeraiah, J. Alloys Compd. 507 (2010) 391.
[8] S. Sanghi, S. Duhan, A. Agarwal, P. Aghamkar, J. Alloys Compd. 488 (2009) 454.
[9] S.P. Singh, R.P.S. Chakradhar, J.L. Rao, B. Karmakar, Physica B 405 (2010) 2157.
[10] C.R. Kesavulu, R.P.S. Chakradhar, R.S. Muralidhara, J.L. Rao, R.V. Anavekar, J. Alloys Compd. 496 (2010) 75.
[11] S.P. Singh, R.P.S. Chakradhar, J.L. Rao, B. Karmakar, J. Alloys Compd. 493 (2010) 256.
[12] M. Subhadra, P. Kistaiah, J. Alloys Compd. 505 (2010) 634.
[13] W.J. Chung, J. Choi, Y.G. Choi, J. Alloys Compd. 505 (2010) 661.
[14] G. Nagarjuna, N. Venkatramaiah, P.V.V. Satyanarayana, N. Veeraiah, J. Alloys Compd. 468 (2009) 466.
[15] R.K. Singh, A. Srinivasan, J. Magn. Magn. Mater. 322 (2010) 2018.
[16] N. Kumar, H. Kishan, A. Rao, V.P.S. Awana, J. Alloys Compd. 502 (2010) 283.
[17] P. Pascuta, G. Borodi, A. Popa, V. Dan, E. Culea, Mater. Chem. Phys. 123 (2010) 767.
[18] A. Ghosh, J. Appl. Phys. 64 (1988) 2652.
[19] A. Pan, A. Ghosh, J. Mater. Res. 17 (2002) 1941.
[20] M. Cherian, M.S. Rao, A.M. Hirt, I.E. Wachs, G. Deo, J. Catal. 211 (2002) 482.
[21] X. Ge, M.M. Zhu, J.Y. Shen, React. Kinet. Catal. Lett. 77 (2002) 103.
[22] F. Amano, T. Yamaguchi, T. Tanaka, J. Phys. Chem. B 110 (2006) 281.
[23] A. Ghosh, B.K. Chaudhuri, J. Non-Cryst. Solids 83 (1986) 151.
[24] A. Ghosh, J. Appl. Phys. 65 (1989) 227.
[25] A. Pan, A. Ghosh, Phys. Rev. B 62 (2000) 3190.
[26] S. Rada, A. Dehelean, M. Stan, R. Chelcea, E. Culea, J. Alloys Compd. 509 (2011) 147.
[27] I. Ardelean, M. Flora, J. Mater. Sci.: Mater. Electron. 13 (2002) 357.
[28] R.P.S. Chakradhar, K.P. Ramesh, J.L. Rao, J. Ramakrishna, J. Phys. Chem. Solids 64 (2003) 641.
[29] R.P.S. Chakradhar, G. Sivaramaiah, J.L. Rao, N.O. Gopal, Spectrochim. Acta Part A 62 (2005) 761.
[30] I. Ardelean, S. Cora, R. Ciceo Lucacel, O. Hulpus, Solid State Sci. 7 (2005) 1438.
[31] M.S. Reddy, G.M. Krishna, N. Veeraiah, J. Phys. Chem. Solids 67 (2006) 789.
[32] I. Ardelean, N. Muresan, P. Pascuta, Mod. Phys. Lett. B 20 (2006) 1607.
[33] I. Ardelean, N. Muresan, P. Pascuta, Mater. Chem. Phys. 101 (2007) 177.
[34] E. Culea, J. Non-Cryst. Solids 223 (1998) 147.
[35] N.K. Mohan, M.R. Reddy, C.K. Jayasankar, N. Veeraiah, J. Alloys Compd. 458 (2008) 66.
[36] C.R. Kesavulu, R.S. Muralidhara, J.L. Rao, R.V. Anavekar, R.P.S. Chakradhar, J. Alloys Compd. 486 (2009) 46.
[37] I. Ardelean, M. Peteanu, V. Simon, S. Filip, M. Flora, S. Simon, J. Mater. Sci. 34 (1999) 6063.
[38] I. Ardelean, M. Peteanu, V. Simon, S. Simon, M. Flora, Phys. Chem. Glasses 41 (2000) 153.
[39] S. Simon, R. Pop, V. Simon, M. Coldea, J. Non-Cryst. Solids 331 (2003) 1.
[40] P. Pascuta, G. Borodi, N. Jumate, I. Vida-Simiti, D. Viorel, E. Culea, J. Alloys Compd. 504 (2010) 479.
[41] A. Dietzel, Glasstech. Berl. 22 (1968) 41.
[42] N. Mehta, R.S. Tiwari, A. Kumar, Mater. Res. Bull. 41 (2006) 1664.
[43] E.R. Shaaban, I.S. Yahia, M. Fadel, J. Alloys Compd. 469 (2009) 427.
[44] V. Kumar, S. Sharma, O.P. Pandey, K. Singh, Solid State Ionics 181 (2010) 79.
[45] A. Hruby, Physica B 22 (1972) 1187.
[46] A. Hruby, Physica B 23 (1973) 1263.
[47] M. Saad, M. Poulin, Mater. Sci. Forum 19–20 (1987) 11.
[48] M.M. Wakkad, E.K. Shokr, S.H. Mohamed, J. Non-Cryst. Solids 265 (2000) 157.
[49] K. Chebli, J.M. Saitter, J. Grenet, A. Hamou, G. Saffarini, Physica B 304 (2001) 228.
[50] H.E. Kissinger, Anal. Chem. 29 (1957) 1702.
[51] T.A. Viglis, Phys. Rev. B 47 (1993) 2882.
[52] D.W. Moon, J.M. Aitken, R.K. MacCrone, G.S. Cieloszky, Phys. Chem. Glasses 16 (1975) 91.
[53] D.L. Griscom, J. Non-Cryst. Solids 40 (1980) 211.
[54] D. Toloman, L.M. Giurgiu, I. Ardelean, Physica B 404 (2009) 4198.
[55] I. Ardelean, S. Filip, J. Optoelectron. Adv. Mater. 5 (2003) 157.
[56] R.K. Singh, A. Srinivasan, J. Non-Cryst. Solids 354 (2008) 3166.
[57] R.K. Singh, A. Srinivasan, J. Magn. Magn. Mater. 321 (2009) 2749.
[58] R.K. Singh, A. Srinivasan, Mater. Sci. Eng. C 30 (2010) 1100.
[59] C.M. Hurd, Contemp. Phys. 469 (23) (1982).
[60] I. Ardelean, M. Peteanu, G. Ilonca, Phys. Status Solidi A 58 (1980) K33.